New Phytologist

Destabilization of interaction between cytokinin signaling intermediates AHP1 and ARR4 modulates *Arabidopsis* development

Vivek Verma[1], Jayaraman Sivaraman[1], Anjil Kumar Srivastava[2], Ari Sadanandom[2] and Prakash P. Kumar[1,3]

[1]Department of Biological Sciences, Faculty of Science, National University of Singapore, 117543 Singapore, Singapore; [2]School of Biological and Biomedical Sciences, Durham University, South Road, Durham, DH1 3LE, UK; [3]Temasek Life Sciences Laboratory, 1 Research Link National University of Singapore, 117604 Singapore, Singapore

Author for correspondence
Prakash P. Kumar
Tel: +65-6516-2859
Email: dbskumar@nus.edu.sg

Received: *23 September 2014*
Accepted: *26 November 2014*

New Phytologist (2015) **206:** 726–737
doi: 10.1111/nph.13297

Key words: Arabidopsis histidine phosphotransfer protein 1 (AHP1), Arabidopsis response regulator 4 (ARR4), cytokinin signaling intermediates, multistep phosphorelay (MSP), plant hormone signaling, structural basis of AHP1-ARR4 interaction, two-component signaling (TCS).

Summary

- Eukaryotic two-component signaling involves the His–Asp–His–Asp multistep phosphorelay (MSP). In *Arabidopsis thaliana*, cytokinin-mediated MSP signaling intermediates include histidine kinases (HKs), histidine phosphotransfer proteins (Hpts) and response regulators (RRs). The structure–function relationship of interaction between Hpt (e.g. AHP1) and RR (e.g. ARR4) is poorly understood.
- Using a homology model and yeast two-hybrid analysis, we identified key amino acids of ARR4 at the AHP1–ΔARR4$^{(16–175)}$ interaction interface. Mutating them in *Arabidopsis* (*arr3,4,5,6,8,9* hextuple mutant background) and performing root length assays provided functional relevance, and coimmunoprecipitation (coIP) assay provided biochemical evidence for the interaction.
- The homology model mimics crystal structures of Hpt–RR complexes. Mutating selected interface residues of ARR4 either abolished or destabilized the interaction. D45A and Y96A mutations weakened interaction with AHP1, and exhibited weaker rescue of root elongation in the hextuple mutants. CoIP analysis using cytokinin-treated transgenic *Arabidopsis* seedlings provided biochemical evidence for weakened AHP1–ARR4 interaction. The relevance of the selected residues for the interaction was further validated in two independent pairs of Hpt–RR proteins from *Arabidopsis* and rice (*Oryza sativa*).
- Our data provide evidence of a link between Hpt–RR interaction affinity and regulation of downstream functions of RRs. This establishes a structure–function relationship for the final step of a eukaryotic MSP signal cascade.

Introduction

Two-component signaling (TCS) systems mediate a wide spectrum of signaling events in prokaryotic and eukaryotic organisms by sensing and responding to various signals. The canonical TCS consists of a membrane-bound sensor histidine kinase (HK) that senses the signals and gets autophosphorylated on the conserved His residue in the kinase domain (Stock *et al.*, 2000). The signal is transmitted as a phosphoryl group to the conserved Asp residue in the receiver domain (RD) of a response regulator (RR). Compared with the prokaryotic TCS systems, the eukaryotic TCS system is more complicated because of the presence of a multistep phosphorelay (MSP) (Appleby *et al.*, 1996). This is necessitated by the presence of RRs in the nucleus while the receptors occur on outer membranes. Therefore, the MSP signaling system follows a sophisticated His–Asp–His–Asp phosphorelay among the multiple signaling intermediates.

The signal transduction pathway of cytokinins, a major class of plant hormones, is an example of the MSP signaling system in plants (To & Kieber, 2008; Hwang *et al.*, 2012). In *Arabidopsis thaliana*, the hybrid sensor kinase family consists of ARABIDOPSIS HISTIDINE KINASE 2 (AHK2), AHK3 and AHK4/CRE1/WOL1, which function as cytokinin receptors (Inoue *et al.*, 2001; Suzuki *et al.*, 2001), AHK1, which is a putative osmosensor (Tran *et al.*, 2007), and CKI1 and AHK5, which are cytokinin-independent HKs (Desikan *et al.*, 2008; Deng *et al.*, 2010). Autophosphorylation of AHKs at the conserved His in the kinase domain initiates MSP, which is then relayed intramolecularly to the conserved Asp in the RD (Hwang *et al.*, 2012). The RD transfers the phosphate group to histidine phosphotransfer proteins (Hpts), namely, the Arabidopsis histidine phosphotransfer proteins (AHPs), which in turn transmit the phosphoryl group to conserved Asp in the RD of Arabidopsis response regulators (ARRs) located mainly in the nucleus. The phosphorylation of ARRs results in their activation, which mediate cytokinin-regulated responses. Two families, namely, type-A and type-B ARRs are involved in this MSP. *Arabidopsis* has 10 type-A ARRs (ARR3-9 and ARR15-17) (Muller & Sheen, 2007), which

are primary transcriptional targets of cytokinin signaling, being rapidly up-regulated upon cytokinin treatment (Hwang & Sheen, 2001). There are 11 type-B ARRs (ARR1, ARR2, ARR10-14 and ARR18-21) that consist of an RD at the N-terminus and a DNA-binding domain at the C-terminus (Hosoda *et al.*, 2002). They are transcriptional activators of cytokinin-regulated genes, including type-A ARRs, thereby functioning as positive regulators of cytokinin signaling (Hwang & Sheen, 2001). Furthermore, in-depth molecular characterization of different cytokinin signaling intermediates helped to identify cognate Hpt, type-A RR and type-B RR proteins in rice (Tsai *et al.*, 2012). Characterization of selected rice RRs has shown that they function in a manner similar to their *Arabidopsis* counterparts (Hirose *et al.*, 2007).

The phosphorylated (activated) type-A ARRs negatively regulate cytokinin signaling, and phosphorylation at the conserved Asp is a prerequisite for their function (Lee *et al.*, 2008). This also highlights that interaction of AHPs with type-A ARRs and phosphorelay from the former to the latter is a critical step for cytokinin signaling cascade. Several studies have validated the interaction and phosphotransfer between AHPs and type-A ARRs using yeast two-hybrid assay and monitoring the transfer of the radioactively labeled PO_4^{3-} group (Imamura *et al.*, 1998; Mira-Rodado *et al.*, 2007).

Structural snapshots of the mechanistic basis of interaction and phosphotransfer between RDs and Hpts were obtained from protein complex crystal structures of TCS intermediaries. Examples are available from organisms belonging to various kingdoms, such as $CheA_3P1{\cdot}P\text{-}CheY_6$ from *Rhodobacter sphaeroides* (Bell *et al.*, 2010), $SLN1_{RD}$-YPD1 and $SLN1_{RD}$-$YPD1{\cdot}Mg^{2+}{\cdot}BeF^{3-}$ from *Saccharomyces cerevisiae* (Xu *et al.*, 2003; Zhao *et al.*, 2008), as well as from the recently published $AHK5_{RD}$–$AHP1{\cdot}Mg^{2+}$ complex from *Arabidopsis* (Bauer *et al.*, 2013). Importantly, the $AHK5_{RD}$–AHP1 complex structure is the first crystal structure of a plant HK_{RD}–Hpt complex. However, it is noteworthy that the two complex structures from eukaryotes mentioned earlier only represent the 'Asp–His' interaction, which corresponds to the middle portion of the His–Asp–His–Asp phosphorelay. The structural details of the final His–Asp step, that is, interaction and phosphotransfer between Hpts and RR_{RD}, have not been studied so far. This could be partly because of the problems associated with the procurement of high yields of recombinant ARR proteins with significant purity (Verma *et al.*, 2013). An alternative approach to address this knowledge gap could be the generation of homology models using available structural information followed by structure–function analysis. A critical comparison of the structures of different RDs, for example, CheY; RR (*Escherichia coli*) (Lee *et al.*, 2001), $SLN1_{RD}$; HK_{RD} (*S. cerevisiae*) (Xu *et al.*, 2003) and $CKI1_{RD}$, $AHK5_{RD}$ (*Arabidopsis*, both are HK_{RD}) (Muller-Dieckmann *et al.*, 1999; Pekarova *et al.*, 2011), revealed that RDs from HKs and RRs possess similar $(\alpha/\beta)_5$ fold across kingdoms. This signifies that the available crystal structures can serve as templates for building computational models of HK_{RD} and RR_{RD}.

In this study, we generated an *in silico* model of AHP1 complexed with the 16- to 175-amino-acid region of ARR4 (henceforth, this region will be referred to as $\Delta ARR4^{(16–175)}$) to interpret the final step (Hpt–RR) of cytokinin signal transduction. Mutations in key amino acid residues of ARR4 identified from the AHP1–$\Delta ARR4^{(16–175)}$ interaction interface resulted in either abolition or weaker interactions with AHP1 in a yeast two-hybrid assay. Interactions of cognate protein pairs from *Arabidopsis* and rice were also tested. *In planta* analyses of two mutants of ARR4, which showed weakened interaction with AHP1, also showed weakened cytokinin signaling. The mutants showed weaker rescue of root elongation, a cytokinin-mediated developmental event, as compared with wild-type (WT) ARR4. Coimmunoprecipitation (coIP) analysis provided a biochemical explanation of the observed differences in root elongation. Our results help to explain the structure–function relationship of the AHP1–ARR4 interaction, which is a critical step in cytokinin signaling.

Materials and Methods

Plant materials and growth conditions

Arabidopsis thaliana (L.) Heynh ecotype Columbia-0 (Col-0) plants were used as the WT control for *in planta* experiments. Plants were grown at 23°C under long-day conditions (16 : 8 h, light : dark). All transgenic plant lines were generated in *arr3,4,5,6,8,9* hextuple mutant background in which six type-A ARRs (*ARR3*, *ARR4*, *ARR5*, *ARR6*, *ARR8* and *ARR9*) were knocked out (To *et al.*, 2004). Seeds of the hextuple mutant (CS25279) were obtained from the Arabidopsis Biological Resource Centre (ABRC) (http://www.abrc.osu.edu).

For seedling assays, the seeds were surface-sterilized and sown on Murashige and Skoog (MS) semisolid medium (Caisson LABS, North Logan, UT, USA) containing 1 × MS, 0.05% 2-(*N*-morpholino)ethanesulfonic acid (MES), 1% sucrose and 0.6% Gelrite™ (Plantmedia, Dublin, OH, USA), unless stated otherwise. They were subsequently stratified at 4°C for 3 d in the dark followed by incubation at 23°C under constant white light (*c.* 50 μmol m^{-2} s^{-1}) (To *et al.*, 2004).

Plasmid construction

Full-length cDNAs encoding AHP1, ARR4, $\Delta ARR4^{(16–175)}$, AHP2, ARR5, OsHP1 and OsRR6 were amplified by PCR and cloned into the pJET vector (Thermo Scientific, Waltham, MA, USA). The various mutant versions of ARR4, ARR5, and OsRR6 were generated by a site-directed mutagenesis approach. All clones were verified by sequencing. For yeast two-hybrid assay, AHP1, AHP2 and OsHP1 were cloned into an HA tag containing $pGADT_7$ (AD) vector (Clontech, Mountain View, CA, USA), whereas ARR4, $\Delta ARR4^{(16–175)}$, ARR5, OsRR6, and all the mutants of ARR4, ARR5 and OsRR6 were cloned into the myc tag containing pGBKT7 (BD) vector (Clontech). For bimolecular fluorescence complementation (BiFC), modified pSAT1 vectors were used in which the expression cassette of pSAT1, including the 35S promoter, and the amino-terminal (N-terminal) or carboxy-terminal (C-terminal) domains of enhanced

yellow fluorescent protein (N-/C-EYFP) were fused to the pGreen binary vector HY105. AHP1 was fused to the C-terminal of C-EYFP, while ARR4, ARR4^{D45A}, and ARR4^{Y96A} were fused to the C-terminal of N-EYFP. For green fluorescent protein (GFP) localization, ARR4, ARR4^{D45A} and ARR4^{Y96A} were fused at the N-terminal of GFP and driven by 35S promoter. For generation of transgenic plants, WT ARR4 and the two mutants were cloned into the pGreen 35S vector possessing an HA tag at the 3′ end.

Generation of transgenic plants

The hextuple mutant (*arr3,4,5,6,8,9*) seeds obtained from ABRC were germinated in soil and PCR-based screening was done to confirm homozygosity and presence of T-DNA inserts in the six genes. The hextuple mutant did not show phenotypic changes compared with the WT. Seeds from homozygous mutant plants were collected and used for subsequent experiments. Transgenic plants were generated by introducing relevant constructs into the hextuple mutant plants via the *Agrobacterium tumefaciens*-mediated floral dip method (Clough & Bent, 1998). Selection was done using BASTA (2 ml l^{-1}) spray followed by genotyping-PCR of the survivors for confirmation. The transgenic lines were taken to T_3 generation for homozygosity before they were used for analyses.

Homology modeling and identification of AHP1–ARR4 contact points

Protein sequences of ΔARR4$^{(16–175)}$ and OsRR6 were submitted to SWISS MODEL (http://www.swissmodel.expasy.org) and the coordinates were generated. The models of the individual proteins were superimposed on the SLN1$_{RD}$–YPD1 complex crystal structure (PDB id: 2R25) (Zhao *et al.*, 2008) using COOT software (Emsley & Cowtan, 2004) to generate the complex model coordinates. Subsequently, these coordinates were energy-minimized. These model coordinates were used to calculate the interaction interface of the two proteins by the CCP4 program.

Yeast two-hybrid assay

The yeast two-hybrid experiment was performed as per the manufacturer's protocol for the Matchmaker GAL4-based two-hybrid system (Clontech). Equal amounts of AD constructs were mixed with the corresponding BD constructs in separate reactions and the mixtures were introduced into the AH109 yeast strain. The transformed yeast cells were selected on Leu$^-$/Trp$^-$/His$^-$ and also on Leu$^-$/Trp$^-$/His$^-$/Ade$^-$ in order to screen for stronger interactions. Aliquots plated on Leu$^-$/Trp$^-$ medium were used as transformation control. Simultaneously, the cells were diluted 1 : 10 and 1 : 100 fold using 0.9% NaCl and plated on Leu$^-$/Trp$^-$ and Leu$^-$/Trp$^-$/His$^-$ media. The plates were incubated for 3–4 d at 30°C and then photographed.

For AHP1 and ARR4 interaction, the presence of both the proteins in the respective yeast cells were detected by Western blot analysis of the transformed cells using anti-HA and anti-myc antibodies (Santa Cruz, Dallas, TX, USA) for AD and BD vector clones, respectively. Total proteins were extracted from overnight yeast cultures (3 ml, with cell density normalized to the culture with lowest OD_{600}) as previously described (Riezman *et al.*, 1983). To ensure equal loading, each extract was subjected to 50% trichloroacetic acid (TCA) precipitation and the resultant protein pellets were resuspended in 100 µl of 2 × sodium dodecyl sulfate (SDS) loading dye before sodium dodecyl sulfate–polyacrylamide gel electrophoresis (SDS-PAGE).

Bimolecular fluorescence complementation

The fusion constructs of C-EYFP:AHP1, N-EYFP:ARR4, N-EYFP:ARR4^{D45A} and N-EYFP:ARR4^{Y96A} were introduced into *Agrobacterium tumefaciens* strain GV3101. The colonies were grown overnight and the next day a 1 ml culture pellet for each construct was resuspended in infiltration buffer (10 mM MES pH 5.6, 10 mM $MgCl_2$, and 100 µM acetosyringone) to get a final OD_{600} of 0.6. Equal volumes of infiltration solution of the pair of constructs to be tested for interaction were mixed and incubated for 3 h at room temperature with gentle shaking. After incubation, leaves from 3-wk-old *Nicotiana benthamiana* Domin plants were infiltrated with the *Agrobacterium* mixture on their abaxial surfaces using a syringe (Walter *et al.*, 2004). The leaves were examined for EYFP signal 3 d postinfiltration using a Carl Zeiss 510 Meta laser scanning confocal microscope (http://www.zeiss.de/axiovert200) with excitation at 514 nm. All images were recorded with the same settings. The signal intensity was measured using ImageJ software (National Institute of Health, Bethesda, MD, USA).

Protoplast isolation and transfection for GFP localization

The protoplasts were extracted from leaves of 3- to 4-wk-old *Arabidopsis* (Col-0) plants (Yoo *et al.*, 2007). For each reaction, *c.* 2 × 10^5 protoplasts were transfected with 15–20 µg of plasmid DNA corresponding to 35S::ARR4-GFP, 35S::ARR4^{D45A}-GFP, 35S::ARR4^{Y96A}-GFP and then incubated for 12–16 h at 25°C in the dark. The GFP signals were monitored by laser scanning microscopy as described earlier, but with excitation at 488 nm. Expression of 35S::GFP was used as a control.

RNA extraction, cDNA synthesis and quantitative real- time PCR (qRT-PCR)

Total RNA was extracted from10-d-old seedlings of WT (Col-0), hextuple mutant and selected transgenic lines of ARR4 and the two mutants using TRIzol® reagent (Life Technologies, Singapore) as per the manufacturer's protocol. Approximately 1 µg of extracted RNA for each sample was used for reverse transcription as per the manufacturer's instructions using the Maxima first-strand cDNA synthesis kit (Thermo Scientific). The 10 µl qRT-PCR reaction mixture included 1 µl cDNA (diluted five-fold), 0.2 µl of each primer, 5 µl 2 × KAPA SYBR® Master Mix (KAPA Biosystems, London, UK) and sterile water. PCR was performed using StepOne™ Real-Time PCR systems (v2.1;

Applied Biosystems, Foster City, CA, USA) and the PCR conditions were as follows: denaturation at 95°C for 20 s; 40 cycles of denaturation at 95°C for 3 s, and annealing and extension at 60°C for 30 s. Amplification of the *TUB2* gene was used as an internal control for normalization. StepOne™ software (v2.1; Applied Biosystems) was used for data analysis from two independent biological replicates.

Root elongation assay

Arabidopsis seedlings were grown in culture Petri plates containing MS medium supplemented with the indicated concentrations of N^6-benzyladenine (BA) or 0.1% dimethyl sulfoxide (DMSO) (solvent). The plates were incubated vertically for 10 d in continuous light (To *et al.*, 2004). The positions of roots were marked on the plates on days 4 and 9 and the plates were photographed on the day 10. The root growth between days 4 and 9 was measured using ImageJ software. Data presented are means ± SE from at least 30 seedlings per transgenic line per treatment with at least two independent transgenic lines for each construct.

ARR7 response to cytokinin treatment

For treatment with cytokinin, the seedlings were grown on horizontal MS plates with 0.5% Gelrite. Ten-day-old seedlings were transferred to 1 × liquid MS supplemented with 50 nM BA, and samples were collected at 0, 30, and 60 min of treatment (To *et al.*, 2004). RNA extraction, cDNA synthesis, and qRT-PCR were performed as described earlier. Expression of *ARR7* was analyzed from two independent biological replicates.

Analysis of protein abundances in transgenic lines

Total protein was extracted from 10-d-old seedlings of the different transgenic lines used for the study using 100 mM Tris HCl (pH 8.0), 150 mM NaCl, 5 mM ethylenediaminetetraacetic acid (EDTA), 5 mM ethylene glycol tetraacetic acid, 10 mM dithiothreitol, 0.5% Triton X-100 and 1 × Complete protease inhibitors (Roche) (To *et al.*, 2007). Protein extracts were separated by SDS-PAGE and transferred to polyvinylidene difluoride (PVDF) membrane (Bio-Rad, Hercules, CA, USA). HA-tagged proteins were detected using anti-HA antibody (Santa Cruz) and visualized with chemiluminescent detection (Thermo Scientific) by autoradiography. Subsequently, the membranes were stained with Ponceau, and a Rubisco protein band was used as loading control.

For examining the protein stability, 10-d-old seedlings were treated with 200 μM cycloheximide for different time points (0, 30, 60, 90, 120 min) and western blot was done as described earlier. Signals were quantified using ImageJ.

CoIP of ARR4-HA, $ARR4^{D45A}$-HA and $ARR4^{Y96A}$-HA using recombinant GST-AHP1

Fourteen-day-old seedlings of one representative transgenic line each of WT ARR4 and two mutant versions of ARR4 were treated with 10 nM BA for 45 min. Subsequently, total protein was extracted in 400 mM sucrose, 50 mM Tris HCl (pH 7.5), 10% glycerol, and 2.5 mM EDTA. Recombinant glutathione S-transferase (GST)-AHP1 was expressed and purified as previously described (Verma *et al.*, 2013), but the GST tag was not cleaved. The protein concentration for recombinant GST-AHP1 and seedling extracts were estimated using the Direct Detect® Spectrometer (Merck Millipore, Billerica, MA, USA). Two micrograms of GST-AHP1 protein were immobilized onto 30 μl of Glutathione Sepharose 4B (GE Healthcare, Chiltern, UK) beads. Subsequently, *c.* 20 μg of seedling protein extracts from representative transgenic lines were added to the immobilized GST-AHP1 in independent reactions and incubated for 2 h at 4°C in the coIP buffer (50 mM Tris HCl, 100 mM NaCl, 10% glycerol, 5 mM EDTA, 0.1% Triton X-100). Subsequently, the beads were washed three times with coIP buffer to remove non-specific binding. Finally, the samples were boiled with 1 × SDS loading buffer for 10 min and subjected to SDS-PAGE. Proteins were transferred to the PVDF membrane (Bio-Rad) and probed with anti-HA (Roche) antibody and reprobed with anti-GST (Sigma, St Louis, MO, USA) antibody.

Results

Generation of a homology model for AHP1–ΔARR4$^{(16–175)}$ complex

In order to understand the structural basis of the AHP1–ARR4 interaction, we generated a homology model for AHP1–ΔARR4$^{(16–175)}$ using the $SLN1_{RD}$–YPD1·$Mg2^{+}$·BeF^{3-}complex crystal structure (PDB id: 2R25) as the template (Zhao *et al.*, 2008). The sequence similarity of AHP1 with YPD1 is *c.* 44% (Fig. 1a). The sequence similarity of the 16- to 175-amino-acid region of ARR4 (putative RD) with the RD (R1; 1086–1221) of SLN1 is *c.* 42% (Fig. 1b). The histidine residue required for phosphotransfer (His79 for AHP1; highlighted in yellow) and all the functionally critical amino acid residues of ARR4, including the two aspartates (Asp41; highlighted in blue and Asp95; highlighted in yellow) and a lysine (Lys147; highlighted in purple) required for phosphorylation, are highly conserved. Further, amino acid 32–172 of ARR4 aligned with $SLN1_{RD}$. This was in agreement with Imamura *et al.* (1998) who depicted that ΔARR4$^{(16–175)}$ was capable of receiving the phosphoryl group from the bacterial Hpt domain under *in vitro* conditions. Together, this prompted us to use ΔARR4$^{(16–175)}$ for subsequent analyses.

For generating the complex model AHP1–ΔARR4$^{(16–175)}$, we employed the crystal structure of AHP1 (PDB id: 4EUK) (Bauer *et al.*, 2013). It consists of six α-helices in which four helices bundle to form a central core (shown in red in Fig. 1c). His79, the conserved histidine required for phosphorylation, extends from one of the helices of the bundle (inset in Fig. 1c). However, for ΔARR4$^{(16–175)}$, a predicted three-dimensional structure was used. The predicted structure depicted a central core of five parallel β-strands enveloped by five α-helices in groups of two and three, giving an $(\alpha/\beta)_5$ topology (shown in green in Fig. 1c). The conserved residues, such as Asp41, Asp95 and Lys147, form a

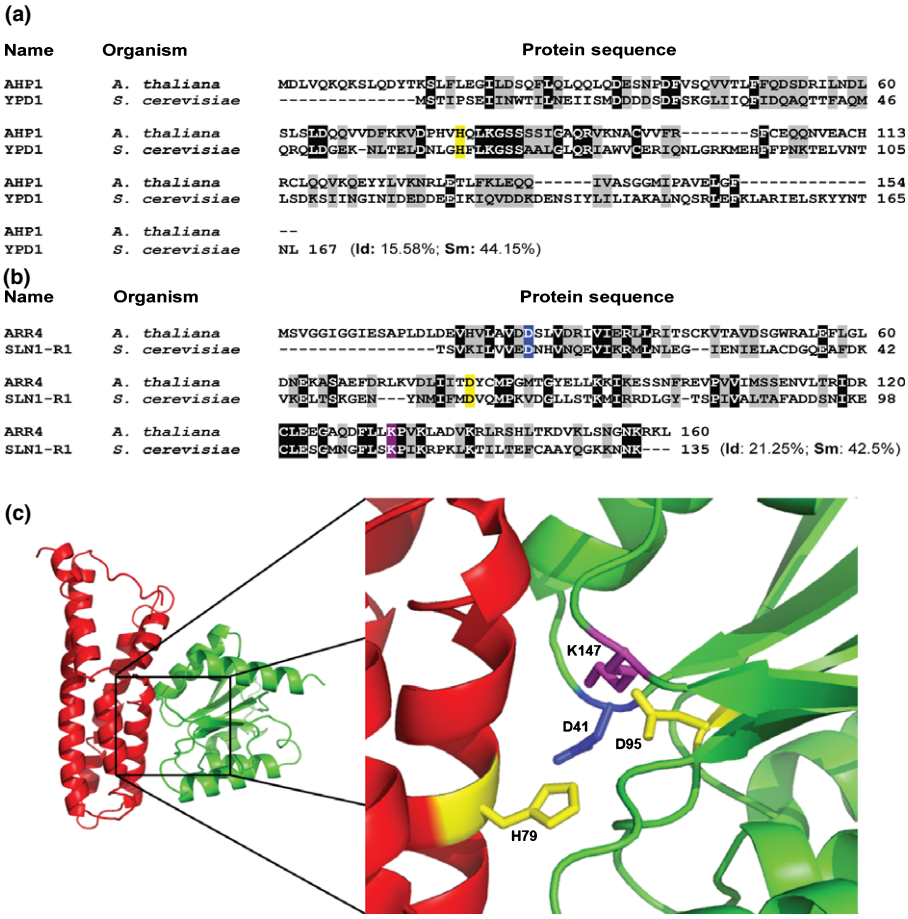

Fig. 1 Generation of a homology model of the AHP1–ΔARR4$^{(16–175)}$ complex of *Arabidopsis thaliana*. (a) Sequence alignment of AHP1 from *A. thaliana* with its homolog from *Saccharomyces cerevisiae*, YPD1. The conserved His required for phosphorylation is highlighted in yellow. (b) Sequence alignment of the 16- to 175-amino-acid region of ARR4 with SLN1$_{RD}$, the receiver domain of *S. cerevisiae* histidine kinase (HK) protein SLN1. The conserved phosphate-binding pocket residues, that is, the two aspartates (in blue and yellow) and lysine (in purple), are highlighted. (c) Overall view of the computational model of the AHP1–ΔARR4$^{(16–175)}$ complex, in which AHP1 is depicted in red and ΔARR4$^{(16–175)}$ is depicted in green. The inset shows a three-dimensional orientation of conserved residues required for phosphorylation, that is, His79 from AHP1, and Asp41, Asp95 and Lys147 from ARR4. Color coding is the same as in sequence alignment (a, b).

pocket (inset in Fig. 1c) that resembles the phosphate-binding pocket of other RRs (Bourret, 2010). Moreover, the $(\alpha/\beta)_5$ fold exhibited by ΔARR4$^{(16–175)}$ model is similar to the structures of other RDs, such as CKI1$_{RD}$ from *Arabidopsis* (PDB id: 3MMN; *c.* 49% sequence similarity) (Pekarova *et al.*, 2011), CheY$_3$ from *Vibrio cholerae* (PDB id: 3TO5; *c.* 46% sequence similarity), AHK5$_{RD}$ from *Arabidopsis* (PDB id: 4EUK; *c.* 39% sequence similarity) (Bauer *et al.*, 2013), and SLN1$_{RD}$ from *S. cerevisiae* (PDB id: 2R25; 27% sequence similarity) (Zhao *et al.*, 2008). The AHP1–ΔARR4$^{(16–175)}$ complex model clearly depicted that residues from the two proteins that are required for phosphotransfer are in close proximity at the interface (inset in Fig. 1c).

AHP1–ΔARR4$^{(16–175)}$ complex model mimics natural Hpt–RR complexes

The computational model of the AHP1–ΔARR4$^{(16–175)}$ complex showed significant alignment with the complex crystal structures of CheA$_3$P1–CheY$_6$ (PDB id: 3KYI; rmsd of 3.2 Å for 191 Cα atoms) (Bell *et al.*, 2010), SLN1$_{RD}$–YPD1 (PDB id: 2R25; rmsd of 1.49 Å for 223 Cα atoms) (Zhao *et al.*, 2008) and AHK5$_{RD}$–AHP1 (PDB id: 4EUK; rmsd of 1.72 Å for 252 Cα atoms) (Bauer *et al.*, 2013) (Fig. 2a). Interestingly, the independent proteins better superimpose than the complex. It indicates possible differences in the relative disposition of the two molecules in the complex compared with the complexes of its homologs. Fig. 2(b) shows the structure-based alignment, which reveals the conserved position of the key amino acids among these structural homologs. Taken together, it suggests that the *in silico* AHP1–ΔARR4$^{(16–175)}$ complex model mimics the natural complexes.

We next investigated if the ΔARR4$^{(16–175)}$ region is functional by examining its ability to interact with AHP1 in the yeast two-hybrid system. Both full-length ARR4 and ΔARR4$^{(16–175)}$ were able to interact with AHP1, because yeast cells harboring AD-AHP1 and BD-ARR4 or BD-ΔARR4$^{(16–175)}$ grew on Leu$^-$/Trp$^-$/His$^-$/Ade$^-$ medium (Fig. 2c). On the contrary, no growth was observed for yeast cells containing empty AD vector with BD-ARR4 or BD-ΔARR4$^{(16–175)}$. Normal growth was observed on Leu$^-$/Trp$^-$, confirming efficient yeast transformation.

Identification of amino acid residues of ARR4 which affect its interaction with AHP1

To identify the key amino acids involved in the AHP1–ARR4 interaction, intermolecular interaction analysis was conducted (< 3.8 Å) with the AHP1–ΔARR4$^{(16–175)}$ complex (Supporting Information, Table S1). Based on this analysis, 12 residues of ARR4 were identified to interact with AHP1, in which five amino acids, namely, Asp45, Arg51, Tyr96, Cys97 and Pro148, have more interactions and were selected for subsequent studies (Fig. 3a shows mapping of these residues on AHP1–ΔARR4$^{(16–175)}$

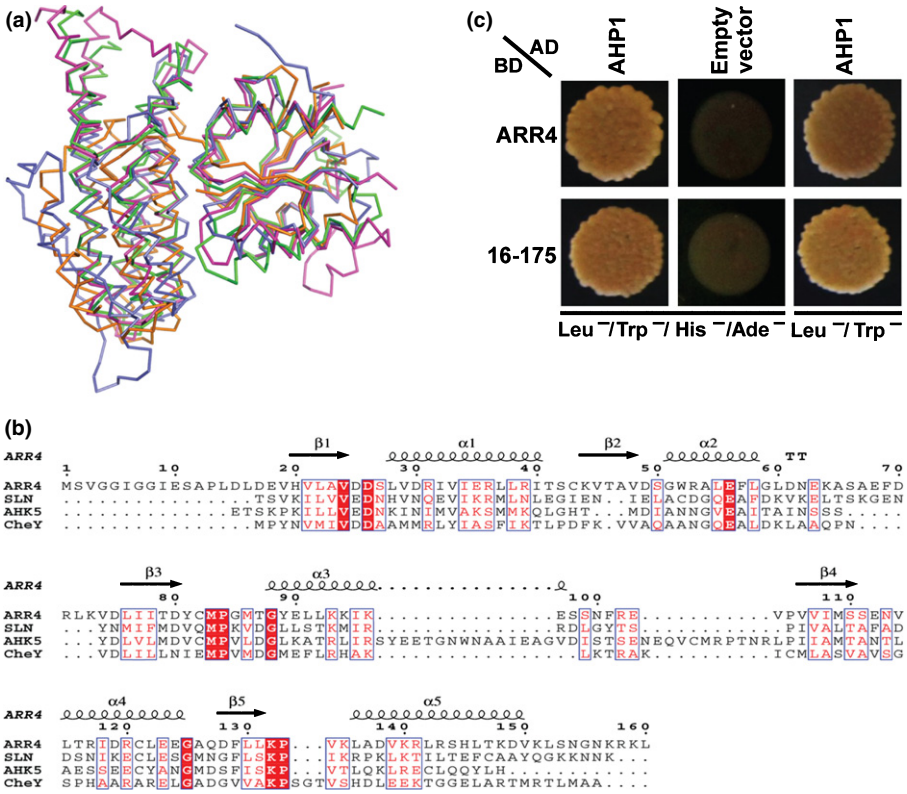

Fig. 2 Validation of the AHP1–ΔARR4$^{(16–175)}$ homology model from *Arabidopsis thaliana* by its comparison with the existing natural complex structures. (a) The Cα superposition of the AHP1–ΔARR4$^{(16–175)}$ (green) *in silico* complex model with its homologs CheA3P1–CheY6 (orange) from *Escherichia coli*, SLN1RD–YPD1 (blue) from *Saccharomyces cerevisiae*, and AHK5RD–AHP1 from *A. thaliana* (magenta). The structural alignment was carried out in PyMol (DeLano, 2002). (b) The structure-based sequence comparison of ARR4 and its homologs. Most of the substitutions are carried with ARR4 and thus we compared its sequences with its structural homologs. The structural alignment was performed using the program COOT (Emsley & Cowtan, 2004). Highly conserved and conserved residues are highlighted. The secondary structures of ARR4 are provided on the top. This figure was prepared using the program ESPript (Gouet *et al.*, 1999). (c) Both full-length ARR4 and ΔARR4$^{(16–175)}$ showed interaction with AHP1 in the yeast two-hybrid system. Growth of yeast cells expressing Gal4 activation domain (AD):AHP1 and Gal 4 DNA-binding domain (BD):ARR4 or BD:ΔARR4$^{(16–175)}$ was examined on selection medium lacking Leu, Trp, His and Ade. Selection medium lacking Leu and Trp was used for checking transformation efficiency. The empty AD vector was used as a negative control.

complex model). It is noteworthy that the selected interacting residues (except Cys97) are conserved among all the 10 members of type-A ARR family (Fig. S1). Cys97 was conserved in six of the 10 members.

To test if the ARR4 amino acid residues selected using *in silico* approaches are indeed involved in the interaction with AHP1, each of the five amino acids was individually mutated to Ala in full-length ARR4. The individual mutants were tested for interaction with AHP1 in the yeast two-hybrid system (Fig. 3b). Full-length WT ARR4 showed significant interaction with AHP1, as the yeast cells harboring the two plasmids grew well on Leu$^-$/Trp$^-$/His$^-$/Ade$^-$. By contrast, ARR4^{D45A}, ARR4^{R51A} and ARR4^{Y96A} mutants showed reduced interaction with AHP1, as yeast cells grew only on Leu$^-$/Trp$^-$/His$^-$ and not on Leu$^-$/Trp$^-$/His$^-$/Ade$^-$. Besides, among the three mutants, the strength of the interaction was in the following sequence, ARR4^{R51A} > ARR4^{Y96A} > ARR4^{D45A}, as revealed by serial dilution (Fig. 3b). However, Cys to Ala mutation at the 97th position had no major impact on ARR4 interaction with AHP1, because ARR4^{C97A} grew on Leu$^-$/Trp$^-$/His$^-$/Ade$^-$. Interestingly, an abolition of interaction between the two proteins was observed with the ARR4^{P148A} mutant. The presence of AHP1, ARR4, and different ARR4 mutant proteins in yeast cells was detected by western blot analysis using anti-HA (for AD:AHP1) and anti-c-myc (for BD:ARR4) antibodies (Fig. 3c).

We further explored the impact of the weakened AHP1–ARR4 interaction on the downstream functions of ARR4 using ARR4^{D45A} and ARR4^{Y96A} mutants. These two mutants showed reduced interaction affinity towards AHP1 in the yeast two-hybrid assays. ARR4^{P148A} was not used, because it led to abolition of interaction. To investigate if the mutations have affected the subcellular localization of the protein, *Arabidopsis* mesophyll protoplasts were transfected with 35S::ARR4-GFP, 35S::ARR4^{D45A}-GFP and 35S::ARR4^{Y96A}-GFP and examined for GFP signals. For all three proteins, namely, WT ARR4, ARR4^{D45A} and ARR4^{Y96A}, we observed a strong signal emerging predominantly from the nucleus, with weak or negligible GFP signal in the cytoplasm (Fig. S2). This clearly revealed that point mutations have not affected the protein localization, as GFP signal of the two mutants overlapped completely with that of WT ARR4. Moreover, the localization pattern of proteins coincides with the published information (Sweere *et al.*, 2001), thereby

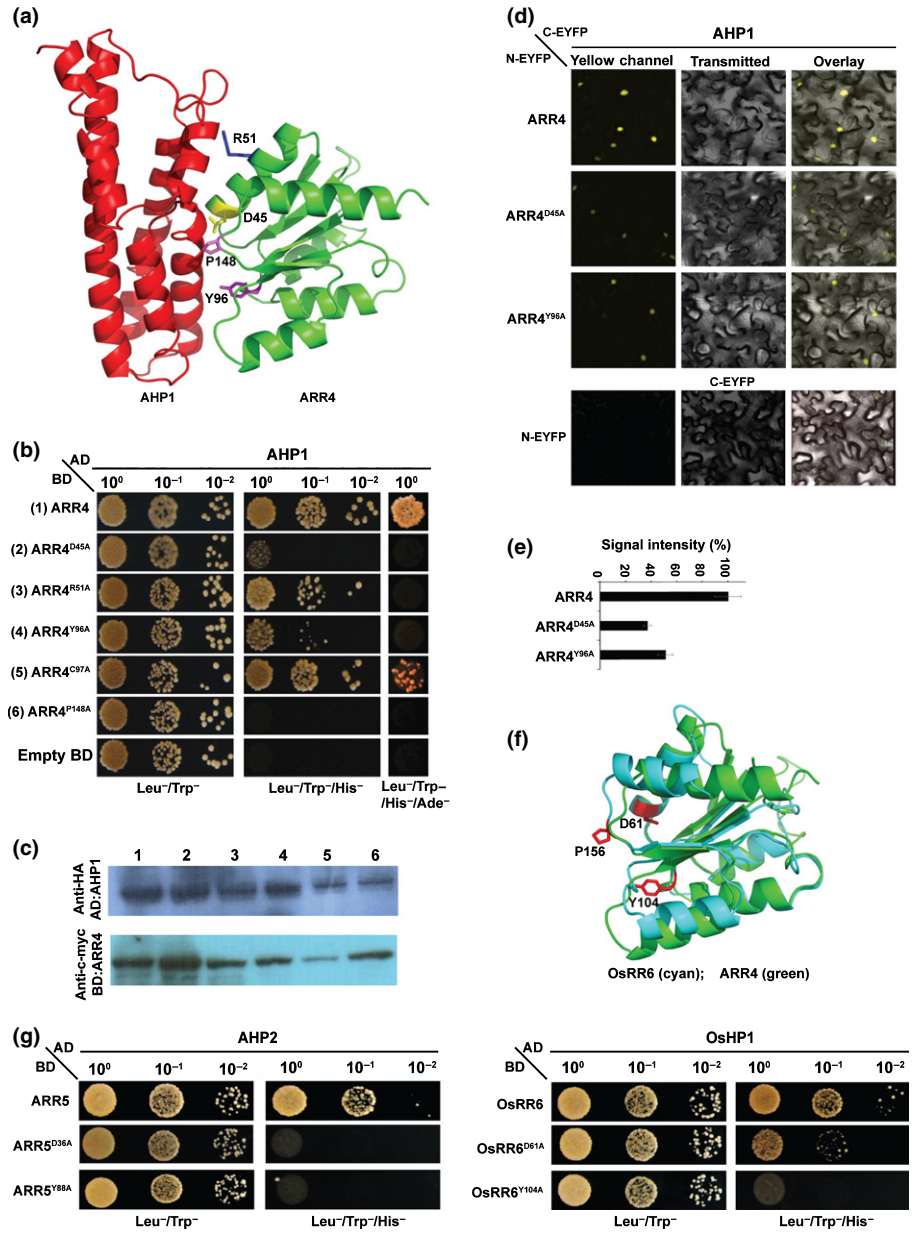

Fig. 3 Identification of *Arabidopsis thaliana* ARR4 residues present at the AHP1–ΔARR4$^{(16–175)}$ complex interface. (a) ARR4 residues Asp45 (yellow), Arg51 (blue), Tyr96 (violet), Cys97, and Pro148 (magenta) mapped onto the AHP1–ΔARR4$^{(16–175)}$ model. Cys97 is not shown for clarity (AHP1, red; ΔARR4$^{(16–175)}$, green). (b) Yeast two-hybrid analysis of Gal 4 activation domain (AD):AHP1 interaction with Gal 4 DNA-binding domain (BD):ARR4 mutants. BD vector was used as the control. No dilution, 10× and 100× dilutions are represented by 10^0, 10^{-1}, and 10^{-2}, respectively. (c) Western blot detection of AD:AHP1 and BD:ARR4 in yeast cells using anti-HA and anti-c-myc antibodies. Line numbers from 1 to 6 correspond to yeast cells harboring AHP1 and ARR4 or different mutants of ARR4, *viz.* ARR4^{D45A}, ARR4^{R51A}, ARR4^{Y96A}, ARR4^{C97A} and ARR4^{P148A}, respectively (similar to the numbering in b). (d) Bimolecular fluorescence complementation (BiFC) interactions of ARR4 and mutants with AHP1. Confocal images of *Nicotiana benthamiana* leaf cells coexpressing C-terminal domain of enhanced yellow fluorescent protein (C-EYFP):AHP1 with either N-EYFP:ARR4 or N-EYFP:ARR4^{D45A}, or N-EYFP:ARR4^{Y96A}. Yellow channel, reconstituted EYFP fluorescence; transmitted, bright-field images; overlay, superimposition of both channels. (e) Relative quantification of the EYFP fluorescence from AHP1 interaction with ARR4, ARR4^{D45A} and ARR4^{Y96A} using ImageJ. Data are means ± SE of signal intensities (28–30 spots per sample), with ARR4 set as 100%. (f) Overlay of the computational model of OsRR6 (cyan) onto ΔARR4$^{(16–175)}$ (green). The Asp45, Tyr96, and Pro148 of ARR4 selected for analysis were also conserved in OsRR6 (Asp61, Tyr104 and Pro156, highlighted in red). (g) Yeast two-hybrid interaction analysis of AD:AHP2 and AD:OsHP1 with wild-type and mutants of BD:ARR5 and BD:OsRR6, respectively. No dilution, 10×, and 100× dilutions are represented by 10^0, 10^{-1} and 10^{-2}, respectively.

further validating our observations. The expression of 35S::GFP was used as the transformation control.

To further verify the weakening of interaction due to mutation of ARR4 at Asp45 and Tyr96 to Ala, ARR4^{D45A} and ARR4^{Y96A} mutants were tested for interaction with AHP1 in *N. benthamiana* leaves using BiFC. The EYFP signals were observed for all three, namely, WT and two variants of ARR4, but the signal intensity was a maximum for ARR4

followed by ARR4^{Y96A} and then ARR4^{D45A} (Fig. 3d,e). This further confirmed that the two proteins were able to interact despite the mutations; however, interaction affinity was in the following declining order, ARR4 > ARR4^{Y96A} > ARR4^{D45A}, thereby validating the yeast two-hybrid results. No signals were observed when the two vectors containing only the EYFP fragments were infiltrated, ensuring that the signals obtained for the AHP1–ARR4 interaction were not due to nonspecific contacts (Fig. 3d).

The selected Asp and Tyr residues of ARR4 were conserved in ARR5 (Fig. S1) as well as in OsRR6, a rice type-A RR (Fig. S3). Further, the superposition of the computational model of OsRR6 onto the ARR4 model clearly showed that the selected residues of OsRR6 exhibit similar three-dimensional orientation to that observed for the corresponding ARR4 residues (Fig. 3f). Hence, to further examine if the mutation of Asp36 and Tyr88 in ARR5 and Asp61, and Tyr104 in OsRR6 can affect the interaction with their corresponding Hpt proteins, we tested the interaction of ARR5, OsRR6 and their mutants with AHP2 and OsHP1, respectively. WT ARR5 and OsRR6 showed significant interaction with AHP2 and OsHP1, respectively, because yeast cells harboring the plasmid pairs showed proper growth on Leu$^-$/Trp$^-$/His$^-$ (Fig. 3g). ARR5^{D36A} or ARR5^{Y88A} did not show any interaction with AHP2. On the other hand, OsRR6^{D61A} showed a weakened interaction with OsHP1 (exhibited by serial dilution), whereas OsRR6^{Y104A} failed to interact with OsHP1. These data further validated the involvement of the selected amino acids in mediating the interaction with Hpts.

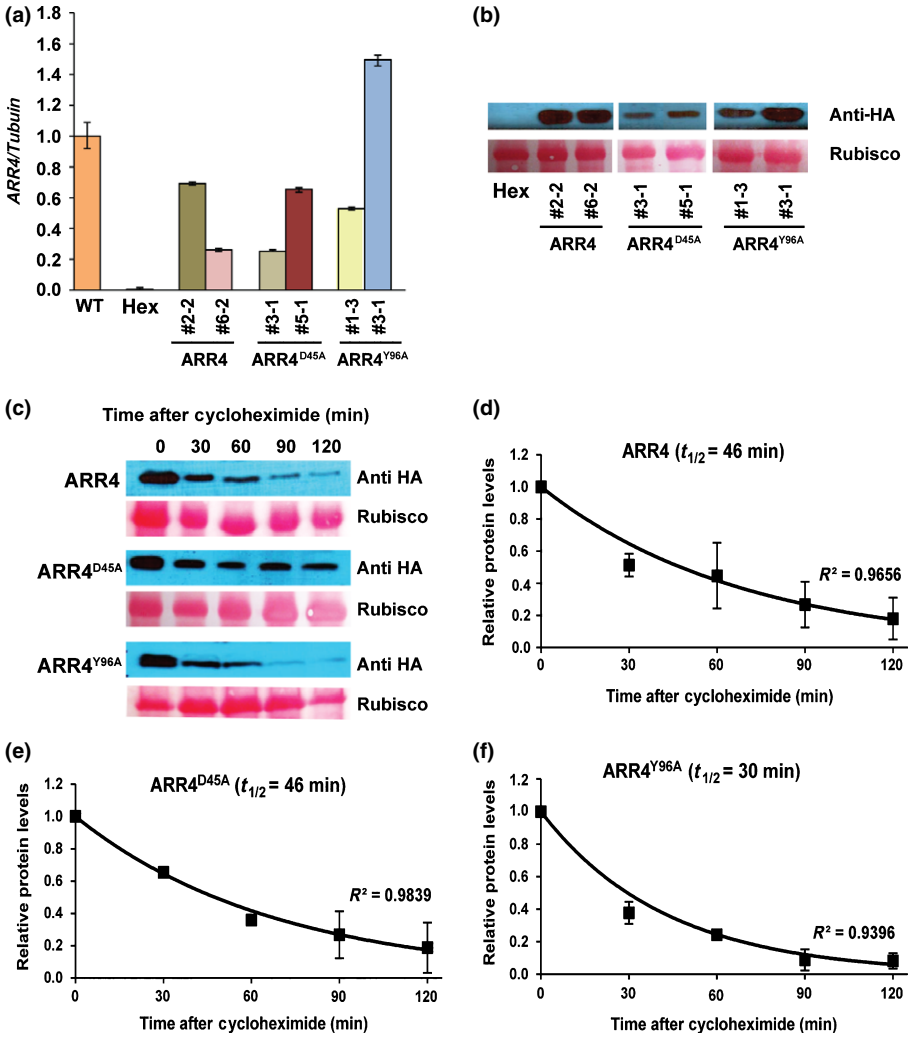

Fig. 4 Detection of relative transcript and protein abundances and analysis of protein turnover rates in transgenic *Arabidopsis thaliana* lines. (a) The transcript abundances of *ARR4*, *ARR4^{D45A}* and *ARR4^{Y96A}* were detected in the different transgenic lines used in the study. Data presented are means ± SD from two independent biological replicates. WT, wild-type (Col-0); Hex, hextuple. (b) The protein abundances of ARR4-HA, ARR4^{D45A}-HA and ARR4^{Y96A}-HA were detected in the respective transgenic lines used for the study. Rubisco protein was used as the loading control. (c) The protein abundances of ARR4-HA, ARR4^{D45A}-HA and ARR4^{Y96A}-HA were detected in 10-d-old seedlings treated with cycloheximide for the indicated time points using anti-HA antibody. One representative line of each transgenic was used for the study. Rubisco protein was used as the loading control. (d–f) Relative protein abundances were normalized to the loading control and to their respective levels at time 0 min. Results from two independent experiments were averaged and shown with error bars representing ± SD. An exponential best-fit curve was fitted through the data points. Correlation coefficient (R^2) values are indicated as a measure of curve fit. The half-life was estimated from the curve assuming first-order kinetics.

D45A and Y96A point mutations did not alter ARR4 protein stability in *Arabidopsis*

As a definitive validation of the functional relevance of weakened AHP1–ARR4 interaction in the native environment, we generated transgenic *Arabidopsis* lines overexpressing 35S::ARR4-HA, 35S::ARR4^{D45A}-HA and 35S::ARR4^{Y96A}-HA in the type-A ARR hextuple mutant (*arr3,4,5,6,8,9*) background (To *et al.*, 2004). For each construct, we generated at least five independent transgenic lines. The hextuple mutant background was chosen to overcome the functional redundancy shown by type-A ARRs (Fig. S4). Two homozygous transgenic lines were selected each for 35S::ARR4-HA (#2-2-ARR4-HA, #6-2-ARR4-HA), 35S::ARR4^{Y96A}-HA (#1-3-ARR4^{Y96A}-HA, #3-1-ARR4^{Y96A}-HA), and 35S::ARR4^{D45A}-HA (#3-1-ARR4^{D45A}-HA, #5-1-ARR4^{D45A}-HA). Comparable abundances of relative *ARR4* transcripts and corresponding proteins were detected in all the selected transgenic lines (Fig. 4a,b).

To test if the mutations have altered the relative protein stability of the HA-tagged fusion proteins *in planta*, we examined the protein turnover rates in one representative transgenic line each for #2-2-ARR4-HA, #3-1-ARR4^{D45A}-HA and #3-1-ARR4^{Y96A}-HA. Detection of relative protein abundances at 30, 60, 90 and 120 min after cycloheximide treatment showed that the protein turnover rates for the three proteins were comparable, thereby confirming that mutations have not affected the stability of the protein (Fig. 4c–f).

D45A and Y96A mutations weakened ARR4-mediated cytokinin response

To investigate the effect of mutations on ARR4-mediated cytokinin functions, we employed the root elongation bioassay, which is one of the best-characterized responses of cytokinin (To *et al.*, 2004). Examination of WT (Col-0) and hextuple mutant seedling roots at 0, 5, 10, 50 and 100 nM BA concentrations showed that the root length of hextuple mutants was significantly inhibited at 5 and 10 nM BA, compared with Col-0 (Fig. S5). Nevertheless, at 50 and 100 nM concentrations, even WT (Col-0) root growth was retarded. The data are consistent with earlier reports (To *et al.*, 2004). Consequently, homozygous transgenic lines corresponding to 35S::ARR4-HA (#2-2-ARR4-HA, #6-2-ARR4-HA,), 35S::ARR4^{D45A}-HA (#3-1-ARR4^{D45A}-HA, #5-1-ARR4^{D45A}-HA), and 35S::ARR4^{Y96A}-HA (#1-3-ARR4^{Y96A}-HA, #3-1-ARR4^{Y96A}-HA) were tested for primary root elongation at 5 and 10 nM BA concentrations (Fig. 5a,b).

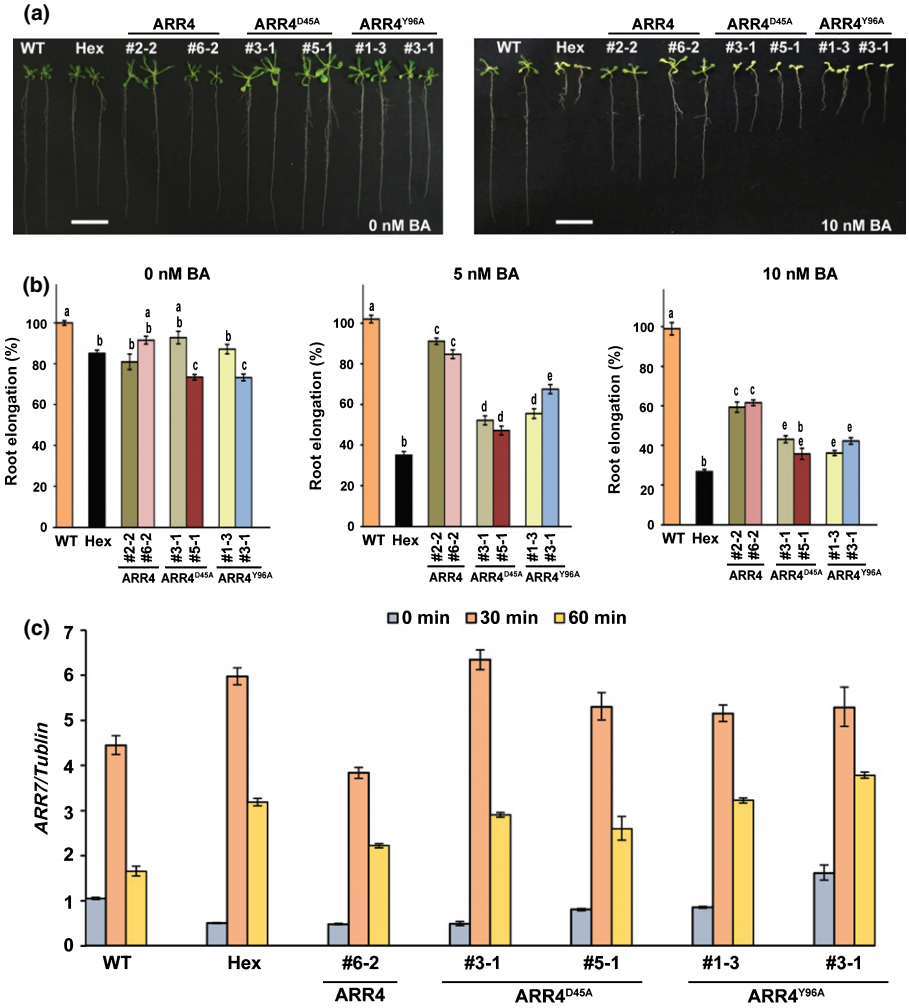

Fig. 5 ARR4^{D45A} and ARR4^{Y96A} showed weaker rescue of hextuple knockout than ARR4 in *Arabidopsis thaliana* root elongation assay and *ARR7* expression in response to exogenous cytokinin. (a) A representative snapshot of the root elongation of *A. thaliana* seedlings corresponding to two independent transgenic lines each of ARR4-HA, ARR4^{D45A}-HA and ARR4^{Y96A}-HA on 0 nM N^6-benzyladenine (BA) and 10 nM BA. (b) The quantification of primary root elongation of two independent transgenic lines for each of the three constructs at 0, 5 and 10 nM BA concentrations. The data represent the means ± SE of primary root growth between days 4 and 9 from at least 30 individual seedlings for each transgenic line at each BA concentration. A two-tailed Student's *t*-test was performed among means of root lengths under each BA concentration. Transgenic lines with different letters were significantly different from others ($P < 0.001$). Bar, 1 cm. (c) Ten-day-old seedlings of wild-type (WT), hextuple mutant (Hex), and different transgenic lines were treated with 50 nM BA for the indicated time points, and *ARR7* expression levels were analyzed. Data are means ± SD from two independent biological replicates and normalized to *TUB2* expression.

An additional transgenic line for each of the three constructs, *viz.* #8-1-ARR4-HA, #4-1-ARR4^{D45A}-HA and #5-1-ARR4^{Y96A}-HA, was also included for the assay (Fig. S6). We observed that in the absence of exogenous cytokinin, that is, 0 nM BA, primary root growth was similar for all seedlings, including WT (Col-0) and hextuple mutants. By contrast, at 5 and 10 nM BA, 35S::ARR4-HA exhibited longer primary roots than the two weaker interacting mutants and the hextuple knockout seedlings.

To further examine the impact of mutations on ARR4 functions, we treated the transgenic seedlings of #6-2-ARR4-HA, #3-1-ARR4^{D45A}-HA, #5-1-ARR4^{D45A}-HA, #1-3-ARR4^{Y96A}-HA and #3-1-ARR4^{Y96A}-HA with 50 nM BA and analyzed the expression levels of *ARR7*, an early cytokinin response gene. To *et al.* (2004) have shown that, upon cytokinin treatment, transcript abundances of *ARR7* were much higher in the hextuple mutant than the WT (Col-0), reaching maximal values at 30 min. This is due to the lack of negative feedback regulation offered by other type-A ARRs. *ARR7* levels were significantly lower in #6-2-ARR4-HA as compared with the hextuple mutant, #3-1-ARR4^{D45A}-HA, #5-1-ARR4^{D45A}-HA, #1-3-ARR4^{Y96A}-HA and #3-1-ARR4^{Y96A}-HA at 30 min of BA treatment (Fig. 5c). This clearly showed that WT ARR4 was able to significantly suppress *ARR7* expression, whereas the two mutants did not significantly suppress *ARR7* transcript abundances. Together, these results highlighted that WT ARR4 was able to rescue the hextuple mutant more efficiently, as compared with the minimal rescue exhibited by the two weak interacting mutants of ARR4.

D45A and Y96A mutations weakened ARR4 binding to AHP1

To investigate if the observed phenotypic differences between the WT and mutant versions of ARR4 can be attributed to the weak interaction between AHP1 and ARR4 mutants, we performed a coIP experiment using recombinant GST-AHP1 and HA-tagged ARR4 from a representative transgenic line for each (#2-2-ARR4-HA, #3-1-ARR4^{D45A}-HA and #3-1-ARR4^{Y96A}-HA). As the phenotypic differences were observed in the presence of cytokinin, 14-d-old seedlings were treated with 10 nM BA for 45 min. GST-AHP1 showed reduced binding to mutated forms of ARR4 compared with the WT ARR4 (Fig. 6). The efficiency of pull-down was in the following declining order, ARR4-HA, ARR4^{Y96A}-HA and ARR4^{D45A}-HA, which is consistent with our yeast two-hybrid and BiFC results (Fig. 3b,e). The coIP data clearly indicate that a tight AHP1–ARR4 binding is critical for efficient progression of cytokinin signaling.

Discussion

Characterization of cytokinin signaling components and analyses of associated transcriptional networks have enhanced our understanding of the molecular functioning of the phosphorelay. Nevertheless, structural knowledge of the key signaling steps is essential for a better understanding of the signaling pathways. Although crystal structures of cytokinin signaling intermediaries, such as CKI$_{RD}$ (Pekarova *et al.*, 2011) and the

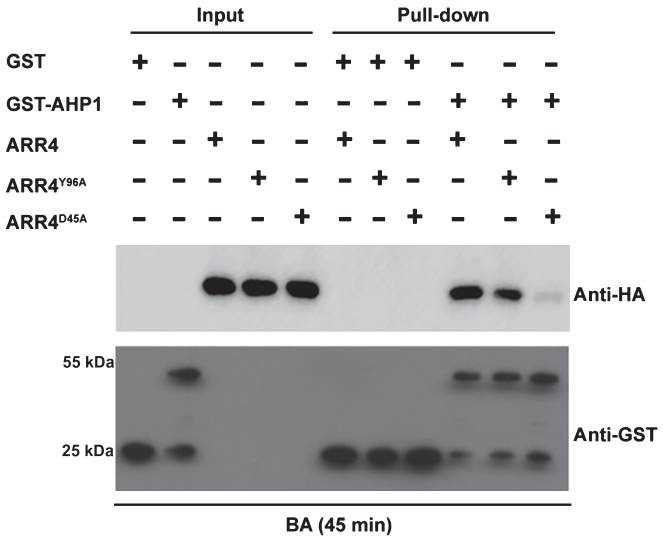

Fig. 6 Coimmunoprecipitation (coIP) of ARR4-HA, ARR4^{D45A}-HA and ARR4^{Y96A}-HA from *Arabidopsis thaliana* with glutathione S-transferase (GST)-AHP1 after cytokinin treatment. Total protein was extracted from 14-d-old cytokinin-treated (10 nM N^6-benzyladenine; BA) seedlings for 45 min of one representative transgenic line for each of the three constructs. The protein was allowed to bind to recombinant GST-AHP1 immobilized on glutathione resin for 2 h. Resin was washed three times and samples were subjected to sodium dodecyl sulfate–polyacrylamide gel electrophoresis (SDS-PAGE) and subsequently probed with anti-HA and anti-GST antibodies. GST protein was used as a control to show the binding specificity of the HA-tagged proteins towards AHP1. Input, the amount of the different proteins at the start of the experiment; pull-down, the amount of proteins detected at the end of the experiment after the washing steps.

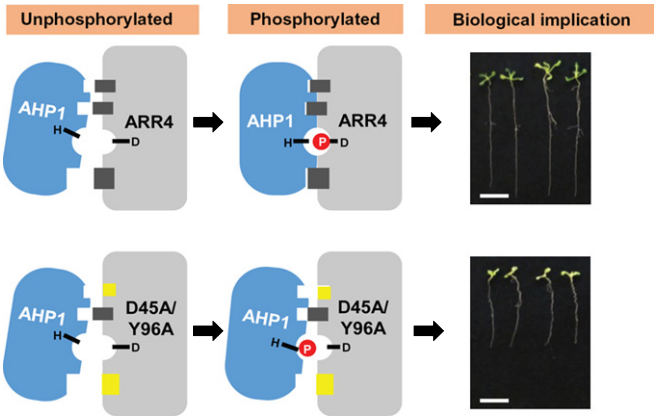

Fig. 7 A schematic representation of the root elongation response mediated by AHP1–ARR4 interaction strength in *Arabidopsis thaliana*. The mechanistic basis of the modification of cytokinin signal strength via AHP1–ARR4 interaction is depicted in the model. H, conserved His79 of AHP1; D, conserved Asp95 of ARR4 (the two amino acids required for phosphorylation). Gray rectangles on ARR4 indicate the amino acid residues at the interaction interface of ARR4 (Asp45, Arg51 and Tyr96) involved in the interaction with AHP1. Two of these rectangles were replaced by yellow boxes in D45A/Y96A to indicate the mutations of Asp45 and Tyr96 to Ala. The red circle harboring P represents the phosphoryl group. Representative photographs of the seedling phenotypes observed are taken from Fig. 5. Bar, 1 cm.

AHK5$_{RD}$–AHP1 complex (Bauer *et al.*, 2013), contributed significantly by providing structural snapshots of the HK$_{RD}$ and mode of phosphotransfer from AHKs to AHPs, the interaction between AHPs and ARRs has not been studied structurally. The fact that transfer of the phosphoryl group from AHPs to type-A ARRs is an essential step for negative regulation of cytokinin signaling further necessitates the structural examination of the interaction. Our study provides a computational model of the AHP1–ΔARR4$^{(16–175)}$ complex and highlights how it can be used to understand the structure–function relationship of the interactions between an Hpt and RR$_{RD}$ in higher eukaryotes.

The AHP1–ΔARR4$^{(16–175)}$ complex model provides significant insights into the mechanistic aspects of interaction between AHP1 with ARR4. It demonstrated that, similar to other Hpt–RD complex structures, the conserved His79 from AHP1 and the 'phosphate-binding pocket' from ARR4 are present in close proximity and hence can efficiently execute the phosphotransfer process (Fig. 1). Model-based identification of amino acid residues of AHP1 from the interaction interface of the AHP1–ΔARR4$^{(16–175)}$ complex revealed the presence of amino acids that are involved in hydrophobic interactions and hydrogen bond formation (Table S1). Furthermore, the destabilization of the AHP1–ARR4 interaction caused by mutations in ARR4 at Asp45, Arg51, Tyr96, Pro148 and Lys150 positions have helped in highlighting the amino acid residues of ARR4 critical for its interaction with AHP1 (Fig. 3). This was substantiated by the destabilization of the AHP2–ARR5 interaction. Furthermore, the OsHP1–OsRR6 interaction was similarly destabilized when the conserved Asp and Tyr residues were mutated (Fig. 3), thereby extending the validity of the study to a monocotyledonous species as well.

The poor rescue of hextuple knockout plants by ARR4^{D45A} and ARR4^{Y96A} in the root elongation assay and *ARR7* expression assay (Fig. 5) clearly indicated that the mutations, besides affecting the interaction ability of ARR4 with AHP1, also perturbed ARR4 functions. The possibility that observed malfunctioning of ARR4 mutants could be due to structural aberrations caused by the mutations was invalidated by the ability of ARR4^{D45A} and ARR4^{Y96A} to interact with AHP1 (Fig. 3), suggesting that mutations had not affected the overall fold of ARR4. Also, predominant nuclear localization of ARR4^{D45A}-GFP and ARR4^{Y96A}-GFP, similar to ARR4-GFP (Fig. S2), showed that mutations had not disturbed the subcellular localization of ARR4. Moreover, comparable protein turnover rates of the WT and mutant forms of ARR4 clearly highlighted that mutations have not affected the stability of the ARR4 protein (Fig. 4).

Our data of weakened interaction between AHP1 and ARR4 leading to altered root elongation response support the view that a close and tight contact between the two signaling intermediates is critical for efficient phosphotransfer and mediating downstream functions. Similarly, earlier studies of SLN1$_{RD}$–YPD1 complex structures of yeast in the absence and presence of Mg^{2+} and BeF^{3-} showed that YPD1 undergoes a rigid-body shift for alignment of conserved His within an ideal distance of, and in linear O-P-N geometry with, conserved Asp of SLN1$_{RD}$ for efficient phosphotransfer (Zhao *et al.*, 2008). Furthermore, substitution of a key Met in bacterial CheY$_6$ at the interface of CheA$_3$P1–CheY$_6$ showed a reduction in interaction and rate of phosphotransfer between them (Bell *et al.*, 2010). The coIP analysis in the present study showed that even after cytokinin treatment, there was only a weak interaction between the mutant versions of ARR4 and AHP1 (Fig. 6), suggesting that this might be occurring *in vivo* as well, and hence the resultant phenotype in ARR4^{D45A} and ARR4^{Y96A} mutants (Fig. 5). Based on this, we can speculate that weaker interaction of ARR4 with AHP1 could result in a slow rate of phosphotransfer, resulting in the altered root elongation phenotype as shown in the model (Fig. 7).

In conclusion, our data provide evidence for a link between the AHP1–ARR4 interaction and ARR4-mediated cytokinin signal progression. These findings highlight the intricacies of the mechanistic basis of phosphoryl group transfer from Hpt to RR and regulatory functions of RRs. Hence, our study establishes a structure–function relationship for the final step of a eukaryotic MSP signal cascade.

Acknowledgements

This work was supported in part by research funding from The Lee Foundation, Singapore and the National Research Foundation, Prime Minister's Office, Singapore under its Competitive Research Programme (CRP award no. NRF-CRP 7-2010-02). V.V. was recipient of a research scholarship from the National University of Singapore during the early part of the study. We thank Ms Vidya Oruganti for her help in generating the homology model. We also acknowledge the efforts of Dr Jobichen Chacko for assistance in analyzing the homology model.

References

Appleby JL, Parkinson JS, Bourret RB. 1996. Signal transduction via the multistep phosphorelay: not necessarily a road less traveled. *Cell* **86**: 845–848.

Bauer J, Reiss K, Veerabagu M, Heunemann M, Harter K, Stehle T. 2013. Structure–function analysis of *Arabidopsis thaliana* histidine kinase AHK5 bound to its cognate phosphotransfer protein AHP1. *Molecular Plant* **6**: 959–970.

Bell CH, Porter SL, Strawson A, Stuart DI, Armitage JP. 2010. Using structural information to change the phosphotransfer specificity of a two-component chemotaxis signalling complex. *Plos Biology* **8**: e1000306.

Bourret RB. 2010. Receiver domain structure and function in response regulator proteins. *Current Opinion Microbiology* **13**: 142–149.

Clough SJ, Bent AF. 1998. Floral dip: a simplified method for *Agrobacterium*-mediated transformation of *Arabidopsis thaliana*. *Plant Journal* **16**: 735–743.

DeLano WL. 2002. *The PyMOL molecular graphics system, version 1.3.* [WWW document] URL http://pymol.sourceforge.net. [accessed 7 November 2011].

Deng Y, Dong HL, Mu JY, Ren B, Zheng BL, Ji ZD, Yang WC, Liang Y, Zuo JR. 2010. Arabidopsis histidine kinase CKI1 acts upstream of HISTIDINE PHOSPHOTRANSFER PROTEINS to regulate female gametophyte development and vegetative growth. *Plant Cell* **22**: 1232–1248.

Desikan R, Horak J, Chaban C, Mira-Rodado V, Witthoft J, Elgass K, Grefen C, Cheung MK, Meixner AJ, Hooley R *et al.* 2008. The histidine kinase AHK5 integrates endogenous and environmental signals in *Arabidopsis* guard cells. *PLoS ONE* **3**: e2491.

Emsley P, Cowtan K. 2004. Coot: model-building tools for molecular graphics. *Acta Crystallographica Section D: Biological Crystallography* **60**: 2126–2132.

Gouet P, Courcelle E, Stuart DI, Metoz F. 1999. ESPript, analysis of multiple sequence alignments in PostScript. *Bioinformatics* **15**: 305–308.

Hirose N, Makita N, Kojima M, Kamada-Nobusada T, Sakakibara H. 2007. Overexpression of a type-A response regulator alters rice morphology and cytokinin metabolism. *Plant and Cell Physiology* **48**: 523–539.

Hosoda K, Imamura A, Katoh E, Hatta T, Tachiki M, Yamada H, Mizuno T, Yamazaki T. 2002. Molecular structure of the GARP family of plant Myb-related DNA binding motifs of the Arabidopsis response regulators. *Plant Cell* **14**: 2015–2029.

Hwang I, Sheen J. 2001. Two-component circuitry in *Arabidopsis* cytokinin signal transduction. *Nature* **413**: 383–389.

Hwang I, Sheen J, Muller B. 2012. Cytokinin signaling networks. *Annual Review of Plant Biology* **63**: 353–380.

Imamura A, Hanaki N, Umeda H, Nakamura A, Suzuki T, Ueguchi C, Mizuno T. 1998. Response regulators implicated in His-to-Asp phosphotransfer signaling in *Arabidopsis*. *Proceedings of the National Academy of Sciences, USA* **95**: 2691–2696.

Inoue T, Higuchi M, Hashimoto Y, Seki M, Kobayashi M, Kato T, Tabata S, Shinozaki K, Kakimoto T. 2001. Identification of CRE1 as a cytokinin receptor from *Arabidopsis*. *Nature* **409**: 1060–1063.

Lee DJ, Kim S, Ha YM, Kim J. 2008. Phosphorylation of *Arabidopsis* response regulator 7 (ARR7) at the putative phospho-accepting site is required for ARR7 to act as a negative regulator of cytokinin signaling. *Planta* **227**: 577–587.

Lee SY, Cho HS, Pelton JG, Yan D, Berry EA, Wemmer DE. 2001. Crystal structure of activated CheY. Comparison with other activated receiver domains. *Journal of Biological Chemistry* **276**: 16425–16431.

Mira-Rodado V, Sweere U, Grefen C, Kunkel T, Fejes E, Nagy F, Schafer E, Harter K. 2007. Functional cross-talk between two-component and phytochrome B signal transduction in *Arabidopsis*. *Journal of Experimental Botany* **58**: 2595–2607.

Muller B, Sheen J. 2007. Advances in cytokinin signaling. *Science* **318**: 68–69.

Muller-Dieckmann HJ, Grantz AA, Kim SH. 1999. The structure of the signal receiver domain of the *Arabidopsis thaliana* ethylene receptor ETR1. *Structure* **7**: 1547–1556.

Pekarova B, Klumpler T, Triskova O, Horak J, Jansen S, Dopitova R, Borkovcova P, Papouskova V, Nejedla E, Sklenar V *et al.* 2011. Structure and binding specificity of the receiver domain of sensor histidine kinase CKI1 from *Arabidopsis thaliana*. *Plant Journal* **67**: 827–839.

Riezman H, Hase T, van Loon AP, Grivell LA, Suda K, Schatz G. 1983. Import of proteins into mitochondria: a 70 kilodalton outer membrane protein with a large carboxy-terminal deletion is still transported to the outer membrane. *EMBO Journal* **2**: 2161–2168.

Stock AM, Robinson VL, Goudreau PN. 2000. Two-component signal transduction. *Annual Review of Biochemistry* **69**: 183–215.

Suzuki T, Miwa K, Ishikawa K, Yamada H, Aiba H, Mizuno T. 2001. The Arabidopsis sensor His-kinase, AHK4, can respond to cytokinins. *Plant and Cell Physiology* **42**: 107–113.

Sweere U, Eichenberg K, Lohrmann J, Mira-Rodado V, Baurle I, Kudla J, Nagy F, Schafer E, Harter K. 2001. Interaction of the response regulator ARR4 with phytochrome B in modulating red light signaling. *Science* **294**: 1108–1111.

To JP, Deruere J, Maxwell BB, Morris VF, Hutchison CE, Ferreira FJ, Schaller GE, Kieber JJ. 2007. Cytokinin regulates type-A *Arabidopsis* response regulator activity and protein stability via two-component phosphorelay. *Plant Cell* **19**: 3901–3914.

To JP, Haberer G, Ferreira FJ, Deruere J, Mason MG, Schaller GE, Alonso JM, Ecker JR, Kieber JJ. 2004. Type-A Arabidopsis response regulators are partially redundant negative regulators of cytokinin signaling. *Plant Cell* **16**: 658–671.

To JP, Kieber JJ. 2008. Cytokinin signaling: two-components and more. *Trends in Plant Science* **13**: 85–92.

Tran LSP, Urao T, Qin F, Maruyama K, Kakimoto T, Shinozaki K, Yamaguchi-Shinozaki K. 2007. Functional analysis of AHK1/ATHK1 and cytokinin receptor histidine kinases in response to abscisic acid, drought, and salt stress in *Arabidopsis*. *Proceedings of the National Academy of Sciences, USA* **104**: 20623–20628.

Tsai YC, Weir NR, Hill K, Zhang W, Kim HJ, Shiu SH, Schaller GE, Kieber JJ. 2012. Characterization of genes involved in cytokinin signaling and metabolism from rice. *Plant Physiology* **158**: 1666–1684.

Verma V, Sivaraman J, Kumar PP. 2013. Expression, purification, and characterization of cytokinin signaling intermediates: Arabidopsis histidine phosphotransfer protein 1 (AHP1) and AHP2. *Plant Cell Reports* **32**: 795–805.

Walter M, Chaban C, Schutze K, Batistic O, Weckermann K, Nake C, Blazevic D, Grefen C, Schumacher K, Oecking C *et al.* 2004. Visualization of protein interactions in living plant cells using bimolecular fluorescence complementation. *Plant Journal* **40**: 428–438.

Xu Q, Porter SW, West AH. 2003. The yeast YPD1/SLN1 complex: insights into molecular recognition in two-component signaling systems. *Structure* **11**: 1569–1581.

Yoo SD, Cho YH, Sheen J. 2007. *Arabidopsis* mesophyll protoplasts: a versatile cell system for transient gene expression analysis. *Nature Protocols* **2**: 1565–1572.

Zhao XD, Copeland DM, Soares AS, West AH. 2008. Crystal structure of a complex between the phosphorelay protein YPD1 and the response regulator domain of SLN1 bound to a phosphoryl analog. *Journal of Molecular Biology* **375**: 1141–1151.

Supporting Information

Additional supporting information may be found in the online version of this article.

Fig. S1 Multiple sequence alignment of ARR4 with other members of the type-A ARR family in *Arabidopsis thaliana*.

Fig. S2 Subcellular localization of GFP fusion proteins of ARR4, $ARR4^{D45A}$, and $ARR4^{Y96A}$ in *Arabidopsis* mesophyll protoplasts.

Fig. S3 Sequence alignment of $\Delta ARR4^{(16–175)}$ of *Arabidopsis thaliana* with rice type-A RR, OsRR6.

Fig. S4 Validation of type-A ARR hextuple knockout in *Arabidopsis thaliana*.

Fig. S5 Hextuple mutants are more sensitive to cytokinin than *Arabidopsis thaliana* wild-type (Col-0).

Fig. S6 Root elongation assay data for additional transgenic lines of *Arabidopsis thaliana* (supplement to Fig. 5).

Table S1 Amino acid residues involved in the AHP1–$\Delta ARR4^{(16–15)}$ interaction at 3.8 Å intermolecular distance in *Arabidopsis thaliana*

Please note: Wiley Blackwell are not responsible for the content or functionality of any supporting information supplied by the authors. Any queries (other than missing material) should be directed to the *New Phytologist* Central Office.